ORIGINAL PAPER

Nano Cr(III) Schiff-base complex supported on magnetic Fe$_3$O$_4$@SiO$_2$: efficient, heterogeneous, and recoverable nanocatalyst for chemoselective synthesis of 1,2-disubstituted benzimidazoles

Sedigheh Azadi[1] · Ali Reza Sardarian[1] · Mohsen Esmaeilpour[2]

Abstract

Novel heterogeneous recoverable Fe$_3$O$_4$@SiO$_2$/Schiff-base/Cr(III) magnetic nanocatalyst has exhibited outstanding performance in the synthesis of 2-aryl-1-(arylmethyl)-1H-benzimidazole products through the chemoselective C-N condensation reaction between o-phenylenediamines and benzaldehydes. The nanocatalyst was synthesized and characterized by FT-IR, XRD, VSM, TGA, EDX, TEM, and FE-SEM methods. The loading amount of Cr in the nanocatalyst was measured at 0.31 mmol/g by ICP analysis. Using the nanocatalyst (0.03 g, 0.93 mol% Cr) coupled with EtOH (3.0 cm^3) as a green solvent at room temperature contributed to an efficient catalytic system for making 1,2-disubstituted benzimidazoles within short reaction times (15–28 min), and with high yields (88–98%). The nanocatalyst was simply separated by an external magnet and reused successfully for seven consecutive cycles with low leaching amount of Cr nanoparticles (NPs) (1.2%). Simple catalytic system, high efficiency in the synthesis of the title products, magnetic property, recyclability, and stability of the Fe$_3$O$_4$@SiO$_2$/Schiff-base/Cr(III) nanocatalyst have set the stage for successful production of 1,2-disubstituted benzimidazoles.

Graphical abstract

Introduction

N-Hetero bicyclic aromatic compounds play a substantial role in the area of organic synthesis, among which 1,2-disubstituted benzimidazoles are of great importance [1]. The chemical characteristic feature of this type of organic compound has made it more prominent in biological purposes as they have shown potential activity as anti-viral [2], anticonvulsant [3], anti-ulcer [4], and anti-bacterial [5] drugs. They also have emerged useful in agricultural [6] and electronic [7] fields, as a ligand in transition metal complexation [8], and as a starting component in organic reactions [9].

✉ Ali Reza Sardarian
  sardarian@shirazu.ac.ir

1 Department of Chemistry, College of Sciences, Shiraz University, Shiraz 71946 84795, Iran

2 Chemistry and Process Engineering Department, Niroo Research Institute, Tehran 14686 17151, Iran

Considering the significance of benzimidazoles in various fields, the different synthetic approaches for the construction of 1,2-disubstituted benzimidazole derivatives have been reported in Fig. 1. The most common and important method is the direct condensation of *o*-phenylenediamines (*o*-PDs) with aldehydes, giving 2-aryl-1-(arylmethyl)-1*H*-benzimidazole derivatives [10] (Fig. 1, path A), N-alkylation/arylation of 2-substituted benzimidazoles [9, 11] (Fig. 1, path B), dehydrogenative coupling of alcohols with aromatic diamines [12, 13] (Fig. 1, path C), coupling-intramolecular nucleophilic addition [14] (Fig. 1, path D), arylaminoarylation/ arylaminoalkylation coupling-reduction cyclisation [15, 16] (Fig. 1, path E), arylamination-condensation cascade process [17] (Fig. 1, path F), aza-Wittig-equivalent C–N bond construction [18] (Fig. 1, path F), oxidative coupling of mono- and disubstituted *o*-PDs [19, 20] (Fig. 1, path G), N-alkylation-reduction condensation [21] (Fig. 1, path H), intramolecular aryl amination [22] (Fig. 1, path I), intramolecular dehydrogenative coupling of *N*,*N'*-dialkyl/diaryl *o*-PDs [19, 23] (Fig. 1, path J) are other synthetic methods of 1,2-disubstituted benzimidazoles.

Regarding the availability and low cost of the substrates, simple operation, and appropriate with safe conditions, the classical and well-known condensation of *o*-PDs with aldehydes is practically used for the synthesis of 2-aryl-1-(arylmethyl)-1*H*-benzimidazoles. The following examples of the catalytic systems illustrate the point in the condensation reaction. Zn-proline [24], Bi(OTf)$_3$ [25], [(CH$_2$)$_4$SO$_3$HMIM][HSO$_4$] [26], AcOH [27], sodium dodecylsulfate [28], LnCl$_3$ [29], nano In$_2$O$_3$ [30], SBA-Pr-SO$_3$H [31], Cu(NO$_3$)$_2$·3H$_2$O [32], aluminosilicate zeolite [33], ZrO$_2$-β-cyclodextrin [34], ZnO/ionic liquid [35], Er(OTf)$_3$ [36], lactic acid [37], Cu(0)/Al$_2$O$_3$ [38], ytterbium/silica [39], nano Co$_3$O$_4$ [40], *p*-toluenesulfonic acid [41], montmorillonite K10 [42], CoFe$_2$O$_4$/Cu(OH)$_2$ [43], and Er(III) cluster [10]. However, many of these reactions suffer from long reaction times, high temperature, poor selectivity, argon/MW irradiation conditions, and a large amount of usage, non-reusability, and air sensitivity of catalyst, which

Fig. 1 Different approaches for the synthesis of 1,2-disubstituted benzimidazoles
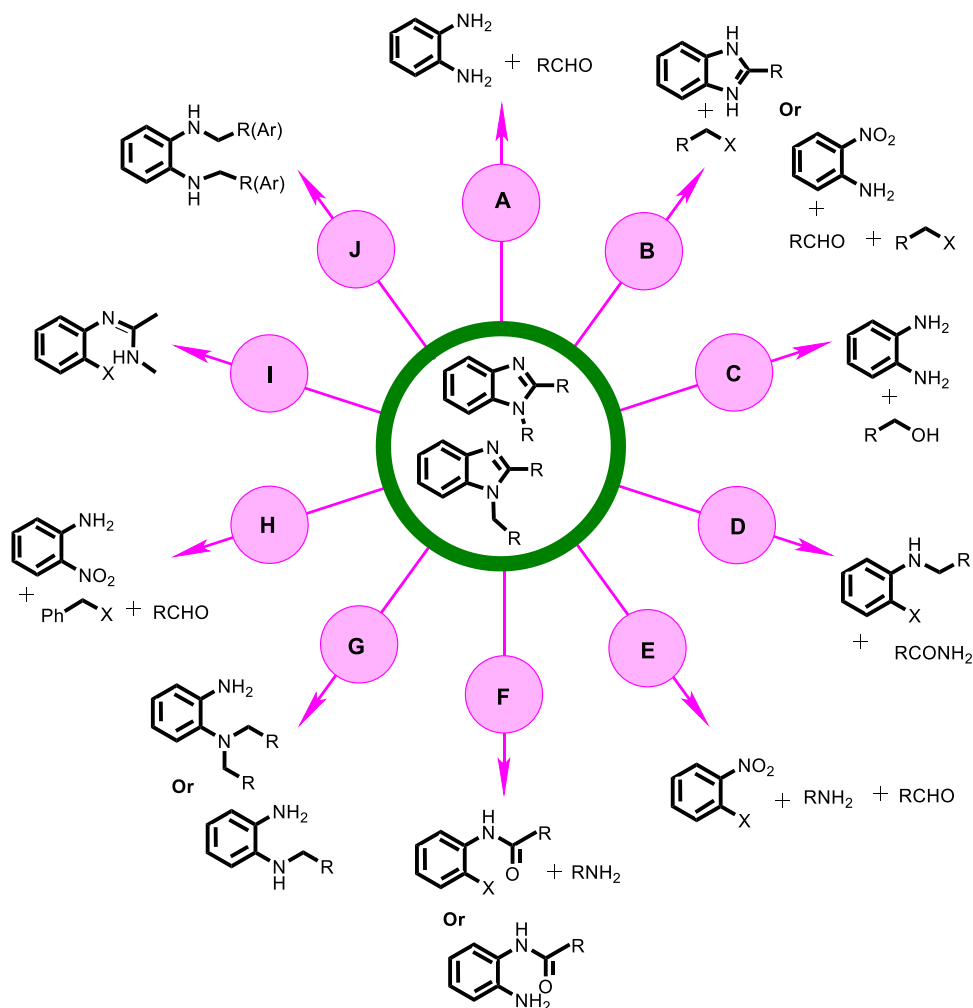
Scheme 1
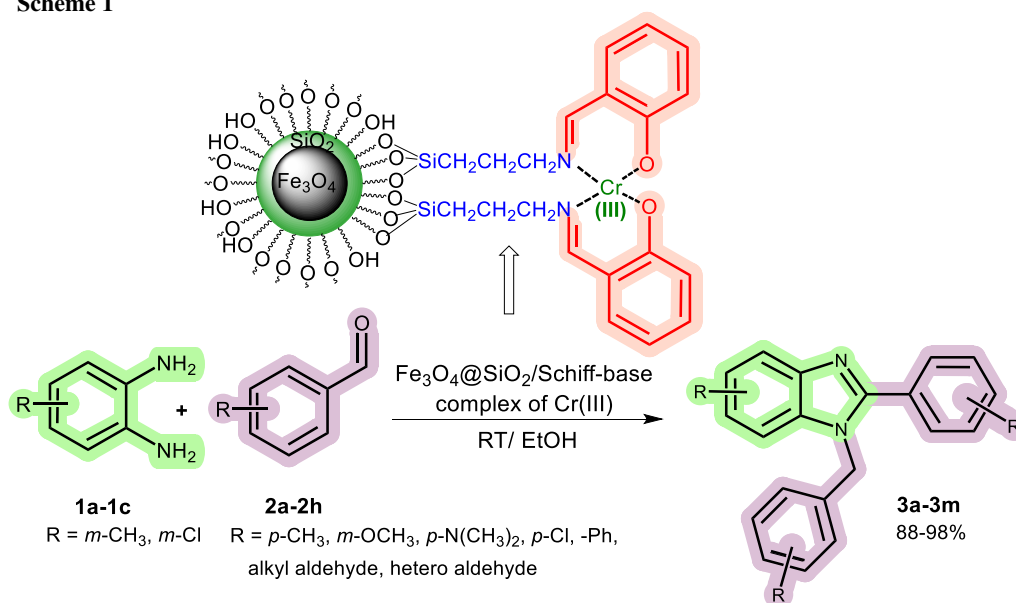
sets the stage for discovering new catalysts to perform much more effectively.

Recently, Fe$_3$O$_4$-based magnetic nanoparticles (MNPs) as heterogeneous catalysts have shown remarkable success in conducting organic reactions, among which Fe$_3$O$_4$ [44] and Fe$_3$O$_4$/chitosan [45] catalyzed the synthesis of 1,2-disubstituted benzimidazole compounds. Moreover, the modification of Fe$_3$O$_4$ NPs not only makes them more chemically stable and compatible but also contributes to different functionalization subsequently [46, 47]. In this regard, silica surface modification gives rise to the synthesis of mesoporous magnetic Fe$_3$O$_4$@SiO$_2$ core–shell, to which various nano metals and Schiff-base complexes can be supported to form heterogeneous nanomagnetic catalysts [46]. Consequently, the efficiency of these nanomagnetic catalysts exerts profound effects on the yield, reaction time, separation, and reusability of the reaction conditions [48].

Fe$_3$O$_4$@SiO$_2$ Schiff-base metal complexes have made significant advances in a wide range of organic reactions, due to the variety in metals used, easy support of Schiff-base complexes on the core–shell structure, high surface-to-volume ratio, high potential ability, environmentally and biocompatibility benign, facile and trouble-free separation [46]. For example, these reactions include the synthesis of 1,1-diacetates [49], Mizoroki–Heck and Suzuki–Miyaura coupling reactions [50], Sonogashira-Hagihara coupling reactions [51], oxidation of alkenes and alcohols [52], synthesis of 2-amino-4H-chromene derivatives [53], N-arylation of α-amino acids and nitrogen-containing heterocycles with aryl halides [54], reduction of aromatic nitro compounds to

aniline derivatives [48], and N-arylation of imidazole with aryl halides [55].

Among various acidic catalysts, Schiff-base complexes of chromium(III) have shown outstanding abilities in catalyzing organic reactions. For example, N-alkylation of amines by alcohols [56], Diels–Alder reaction of 1-amino-3-siloxy-dienes [57], three-component [4 + 2]/allylboration [58], and cross-coupling of phenols [59]. Considering all mentioned above and the importance of a facile and environmentally-friendly method for the synthesis of 2-aryl-1-(arylmethyl)-1H-benzimidazoles, we wish to develop the first procedure using Fe$_3$O$_4$@SiO$_2$ supported Schiff-base complex of Cr(III) as an efficient and magnetically separated nanocatalyst and ethanol as an environmentally green solvent at room temperature for the condensation reaction (Scheme 1).

Results and discussion

This study was initiated by the synthesis process of the Fe$_3$O$_4$@SiO$_2$/Schiff-base/Cr(III) nanocatalyst (Scheme 2). In the first step, the Fe$_3$O$_4$ NPs were made through the mixing of Fe(II) and Fe(III) chloride salts, followed by treatment with tetraethyl orthosilicate (TEOS) as a silica source material under pH control condition to make Fe$_3$O$_4$@SiO$_2$ nano core–shell sphere. In the next step, the Schiff-base ligand having been prepared from salicylaldehyde and (3-amino-propyl)triethoxysilane (APTES) was reacted with Cr(III) metal leading to the Schiff-base complex of Cr(III). Finally, the magnetically heterogeneous Fe$_3$O$_4$@SiO$_2$/Schiff-base/

Scheme 2
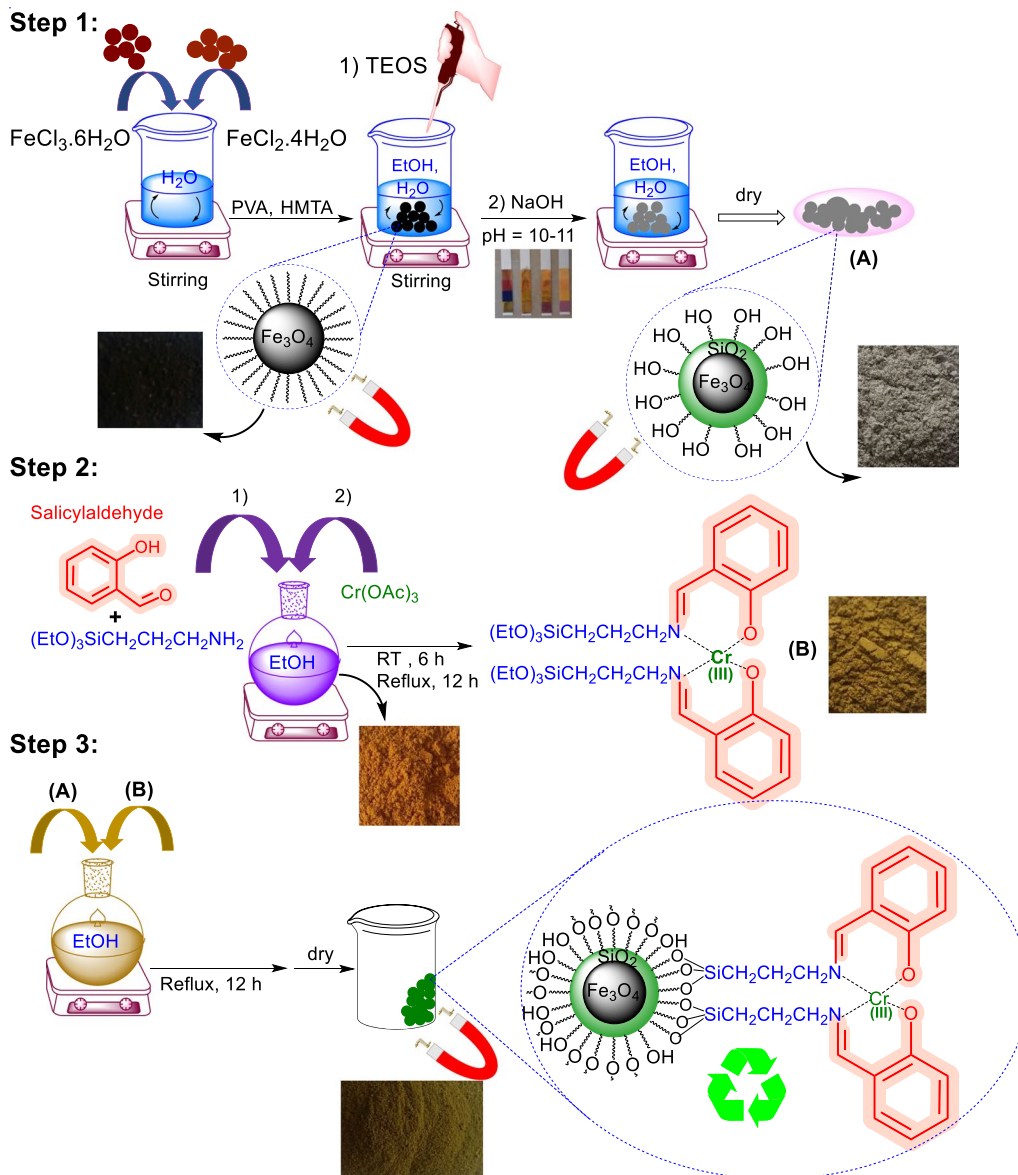

Cr(III) nanocatalyst was obtained by supporting the Schiff-base complex of Cr(III) on the surface of $Fe_3O_4@SiO_2$ NPs (Scheme 2).

The structure of the $Fe_3O_4@SiO_2$/Schiff-base/Cr(III) nanocatalyst was characterized by quantitative and qualitative analyzing methods including Fourier Transform-Infrared Spectroscopy (FT-IR), X-ray Diffraction (XRD) analysis, Vibrating Sample Magnetometer (VSM) technique, Thermogravimetric Analysis (TGA), Transmission Electron Microscopy (TEM), Field Emission Scanning Electron Microscopy (FE-SEM), Energy-dispersive X-ray (EDX) spectroscopy, Dynamic Light Scattering (DLS) technique, Brunauer–Emmett–Teller (BET) analysis, and Inductively Coupled Plasma (ICP) method.

The FT-IR spectra of (a) Fe_3O_4, (b) $Fe_3O_4@SiO_2$, (c) Schiff-base ligand, (d) Schiff-base complex of Cr(III), and (e) $Fe_3O_4@SiO_2$/Schiff-base/Cr(III) identify the specific chemical bonds (Fig. 2). The vibration bands at 516 and 570 cm^{-1} belong to Cr–O and Fe–O bonds, respectively (Fig. 2a and e). The characteristic band of Si–O–Si appears at 1200 cm^{-1} in $Fe_3O_4@SiO_2$ (Fig. 2b), which shifts to 1170 cm^{-1} in the nanocatalyst structure (Fig. 2e). The obvious stretch band at 1634 cm^{-1} is related to the C=N bond in the Schiff-base ligand (Fig. 2c). This band is shifted to the lower frequency at 1622 cm^{-1} due to the coordination of the nitrogen with Cr(III) metal ion in the Schiff-base complex of Cr(III) (Fig. 2d), and the nanocatalyst (Fig. 2e) [49]. Also, the band at 2550 cm^{-1} ascribed to the hydrogen

Fig. 2 FT-IR spectra of **a** Fe_3O_4, **b** Fe_3O_4@SiO_2, **c** Schiff-base ligand, **d** Schiff-base/Cr(III), and **e** Fe_3O_4@SiO_2/Schiff-base/Cr(III); XRD patterns of **f** Fe_3O_4, **g** Fe_3O_4@SiO_2, and **h** Fe_3O_4@SiO_2/Schiff-base/Cr(III)
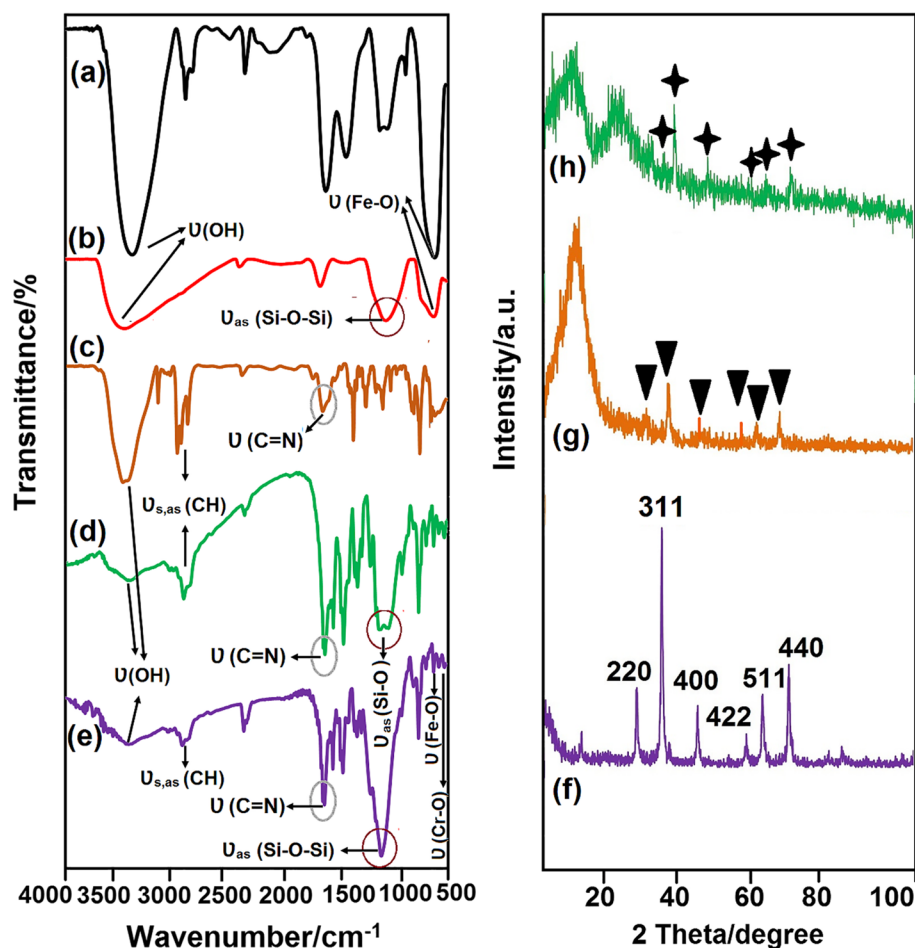
bond between azomethine nitrogen and phenolic hydrogen in the Schiff base ligand structure (Fig. 2c) disappears in the Schiff-base complex of Cr(III) (Fig. 2d), and the nanocatalyst (Fig. 2e), which confirms the complexation of Cr(III) with the ligand. This obvious evidence has justified the synthesis of Fe_3O_4@SiO_2/Schiff-base/Cr(III).

The XRD spectra of (f) Fe_3O_4, (g) Fe_3O_4@SiO_2, and (h) Fe_3O_4@SiO_2/Schiff-base/Cr(III) are depicted in Fig. 2. The six characteristic patterns at $2\theta = 30.2°$, 35.42°, 43.14°, 53.43°, 62°, and 65.62° related to indices 220, 311, 400, 422, 511, and 440, respectively, show crystallographic spinel structure in the Fe_3O_4 NPs (Fig. 2f) [49]. These peaks with lower intensities are also presented in the Fe_3O_4@SiO_2 (Fig. 2g), and Fe_3O_4@SiO_2/Schiff-base/Cr(III) (Fig. 2h) structures as well, which shows the successful wrapping of the Fe_3O_4 NPs with SiO_2 and Schiff base complex of Cr, subsequently. Also, the coated amorphous silica on the surface of Fe_3O_4 NPs gives rise to an obvious diffusion peak at $2\theta = 15–25°$ in Fe_3O_4@SiO_2 (Fig. 2g) [48]. This peak shifts to lower angles by the immobilization of the Schiff-base complex of Cr(III) on the Fe_3O_4@SiO_2 core–shell NPs (Fig. 2h). This observation confirms the successful anchoring of the Schiff base complex of Cr on the surface

of magnetic Fe_3O_4@SiO_2 NPs without affecting the structure of Fe_3O_4 NPs.

The supermagnetic properties of Fe_3O_4, Fe_3O_4@SiO_2, and Fe_3O_4@SiO_2/Schiff-base/Cr(III) NPs were examined by VSM analysis at room temperature. The study was conducted by applying a magnetic field up to 8000 Oe at 300 K (Fig. 3a–c). Almost neither coercivity nor remanence was observed in the magnetization curves of the MNPs, which confirms the superparamagnetic identity of the synthesized NPs. The saturation magnetization (Ms) values were obtained at 67.7 (Fig. 3a) [48], 42.6 (Fig. 3b) [48], 33.6 (Fig. 3c) emu/g for the Fe_3O_4, Fe_3O_4@SiO_2, and Fe_3O_4@SiO_2/Schiff-base/Cr(III), respectively. The decrease in the Ms values of Fe_3O_4@SiO_2 (Fig. 3b), and Fe_3O_4@SiO_2/Schiff-base/Cr(III) (Fig. 3c) compared to the one in Fe_3O_4 (Fig. 3a) is related to the coating of SiO_2 core–shell followed by the immobilization of the Schiff-base complex on the surface of the bared Fe_3O_4 NPs. However, the superparamagnetic behavior remains in the Fe_3O_4@SiO_2/Schiff-base/Cr(III) nanocatalyst (Fig. 3c). This evidence is completed by practical observation in which the nanocatalyst is affected by an external magnetic
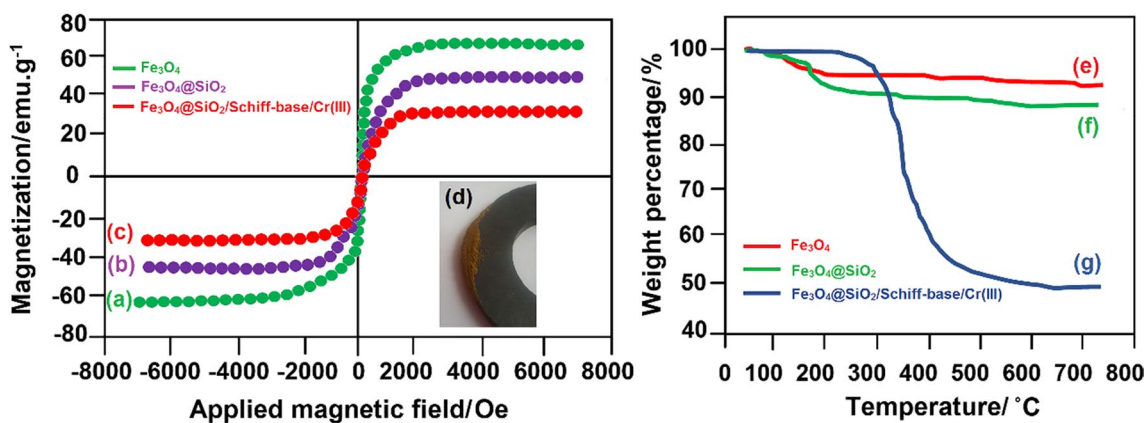
Fig. 3 Magnetic curves of **a** Fe_3O_4, **b** $Fe_3O_4@SiO_2$, and **c** $Fe_3O_4@SiO_2$/Schiff-base/Cr(III); **d** magnetic characteristic image of $Fe_3O_4@SiO_2$/Schiff-base/Cr(III); TGA spectra of **e** Fe_3O_4, **f** $Fe_3O_4@SiO_2$, and **g** $Fe_3O_4@SiO_2$/Schiff-base/Cr(III)

field resulting also in easy separation from the reaction mixture (Fig. 3d).

TGA analysis was used to determine the thermal stability and the fraction of volatile components of the Fe_3O_4, $Fe_3O_4@SiO_2$, and $Fe_3O_4@SiO_2$/Schiff-base/Cr(III) NPs over the temperature range of 25–750 °C (Fig. 3e–g). The thermal decomposition curves show two areas in which the weight loss of NPs occurs. The first one belongs to the loss of surface water and remaining organic solvents in the temperature range of 50–150 °C [54]. In particular, this region for the Fe_3O_4 (Fig. 3e) and $Fe_3O_4@SiO_2$ (Fig. 3f) adsorbing hydroxyl groups and humidity is the major one. The latter occurred between 150 and 600 °C and is likely related to the decomposition of organic compounds. However, the Fe_3O_4 and $Fe_3O_4@SiO_2$ NPs exhibit excellent thermal stability at extreme temperatures. Also, an obvious decrease observed in the weight of $Fe_3O_4@SiO_2$/Schiff-base/Cr(III) nanocatalyst not only shows the successful immobilization of the Schiff-base complex but also displays good thermal stability almost up to the 400 °C (Fig. 3g). This observation confirms the heat resistance of the nanocatalyst at higher temperature conditions.

The elemental composition of $Fe_3O_4@SiO_2$ and $Fe_3O_4@$ SiO_2/Schiff-base/Cr(III) NPs were determined by EDX analysis (Fig. 4). The elemental characterization peaks in $Fe_3O_4@SiO_2$ confirm the efficient silica coating of Fe_3O_4 NPs, which is verified by the higher amount of Si element (Fig. 4a) [54]. As shown in Fig. 4b, the presence of C, N, and Cr elements along with Fe, O, and Si ones demonstrates the successful functionalization of $Fe_3O_4@SiO_2$ core–shell with the Schiff-base complex of Cr, and the synthesis of $Fe_3O_4@$ SiO_2/Schiff-base/Cr(III) nanocatalyst, subsequently.

The structure, morphology, and particle size of Fe_3O_4, $Fe_3O_4@SiO_2$, and $Fe_3O_4@SiO_2$/Schiff-base/Cr(III) NPs were further studied by TEM, FE-SEM, and DLS (Fig. 5). The TEM micrograph of the Fe_3O_4 NPs shows a uniform structure with dark spots of 10–15 nm in average size (Fig. 5a) [49]. The dark Fe_3O_4 NPs are modified by the gray layers of silica in the $Fe_3O_4@SiO_2$ NPs with a thickness of 6–8 nm resulting also in a uniform pattern of NPs with an average size of 20–22 nm (Fig. 5b) [49]. The more densely dark NPs indicate the functionalization of $Fe_3O_4@$ SiO_2 NPs with the Schiff-base complexes of Cr contributing to the well-shaped structure for $Fe_3O_4@SiO_2$/Schiff-base/Cr(III), in which the NPs are dispersed well with a mean

Fig. 4 EDX spectra of **a** $Fe_3O_4@SiO_2$, and **b** $Fe_3O_4@$ SiO_2/Schiff-base/Cr(III)
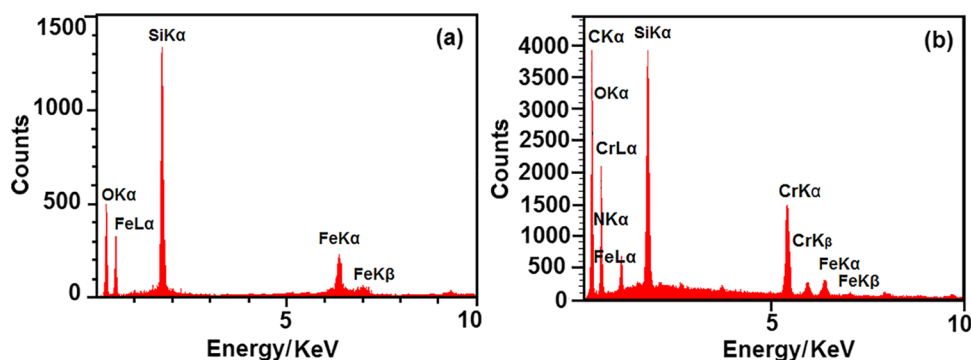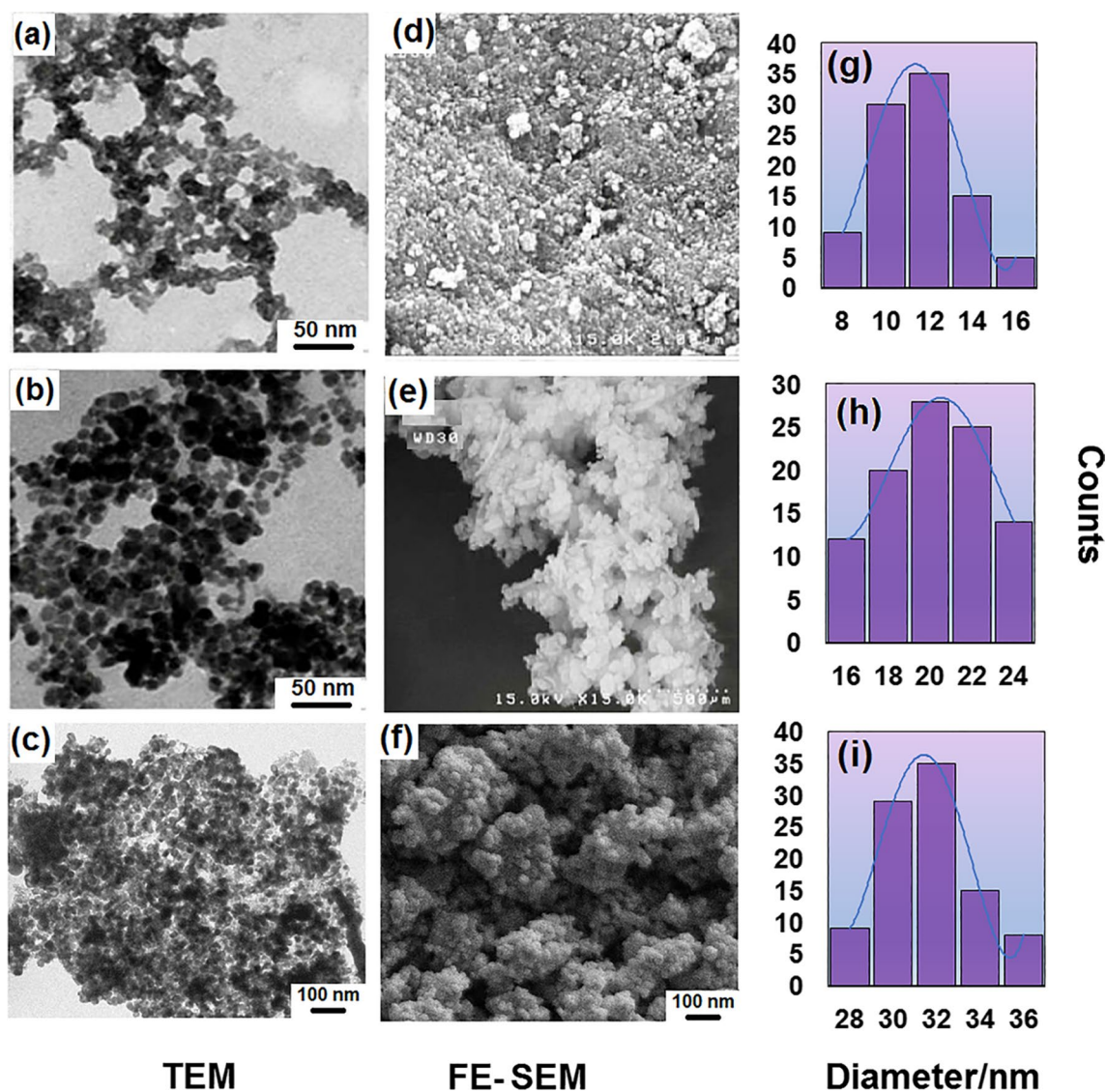
Fig. 5 TEM images of **a** Fe$_3$O$_4$, **b** Fe$_3$O$_4$@SiO$_2$, and **c** Fe$_3$O$_4$@SiO$_2$/Schiff-base/Cr(III); FE-SEM images of **d** Fe$_3$O$_4$, **e** Fe$_3$O$_4$@SiO$_2$, and **f** Fe$_3$O$_4$@SiO$_2$/Schiff-base/Cr(III); particle size distributions of **g** Fe$_3$O$_4$, **h** Fe$_3$O$_4$@SiO$_2$, and **i** Fe$_3$O$_4$@SiO$_2$/Schiff-base/Cr(III)

size of 30–35 nm (Fig. 5c). The FE-SEM image of Fe$_3$O$_4$ NPs shows the spherical morphology of the surface structure (Fig. 5d) [51]. This harmonic surface topography remains in the Fe$_3$O$_4$@SiO$_2$ (Fig. 5e) [51], and Fe$_3$O$_4$@SiO$_2$/Schiff-base/Cr(III) MNPs (Fig. 5f), which represents the successful surface modification of Fe$_3$O$_4$ NPs. DLS analysis was used to measure the size distribution profile of NPs. The average sizes of 12, 20, and 30 nm were determined for the Fe$_3$O$_4$ (Fig. 5g) [49], Fe$_3$O$_4$@SiO$_2$ (Fig. 5h) [49], and Fe$_3$O$_4$@SiO$_2$/Schiff-base/Cr(III) MNPs (Fig. 5i), respectively.

The specific surface areas of MNPs were calculated by Brunauer–Emmett–Teller (BET) method. The measured values were 480 [51], 430.3 [51], and 384.5 m^2/g for Fe$_3$O$_4$, Fe$_3$O$_4$@SiO$_2$, and, Fe$_3$O$_4$@SiO$_2$/Schiff-base/Cr(III), respectively. The gradual decrease in the values could be related

to the silica modification and Schiff-base complex immobilization on the surface of Fe$_3$O$_4$ MNPs. Furthermore, the Cr loading amount of the Fe$_3$O$_4$@SiO$_2$/Schiff-base/Cr(III) nanomagnetic catalyst was determined by the ICP analyzer. The content of Cr in the as-prepared decomposed catalyst in HCl (37%) was obtained at 0.31 mmol/g.

Having been synthesized and characterized, the Fe$_3$O$_4$@SiO$_2$/Schiff-base/Cr(III) nanomagnetic catalyst was applied to evaluate its efficiency and potential activity in the condensation reaction of *o*-PDs and arylaldehydes to produce 2-aryl-1-(arylmethyl)-1*H*-benzimidazoles. In advance, the optimum reaction conditions make the first step to determine the suitable solvent, temperature, the amount of nanocatalyst and divert the reaction selectivity to the desired 1-benzyl-2-phenyl-1*H*-benzo[*d*]imidazole

(**3a**) rather than the 2-phenyl-1*H*-benzimidazole (**4a**). The *o*–PD (**1a**, 1.0 mmol, 0.11 g) and benzaldehyde (**2a**, 2.0 mmol, 0.2 cm^3) as the model substrates, ethanol (EtOH, 3.0 cm^3) as the solvent, and room temperature conditions (RT) were selected to initiate the optimization. First, the condensation reaction did not show selectivity between **3** and **4a** in the absence of the nanocatalyst, and **3a** was obtained with a 45% yield (Table 1, entry 1). Increasing the amount of the nanocatalyst from 0.01 (0.31 mol% Cr) to 0.02 g (0.62 mol% Cr) not only decreases the reaction

Table 1 Evaluation of reaction parameters (solvents, temperature, the amount of nanocatalyst) in the synthesis of 1-benzyl-2-phenyl-1*H*-benzo[*d*]imidazole (**3a**)
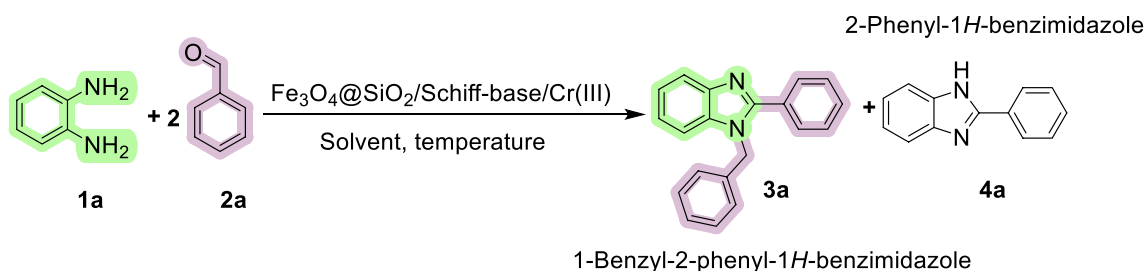
Entry	Catalyst/g, mol% Cr	Solvent/cm^3	Temp./°C	Time/h	Selectivity 3a:4a	Yield/%[a]
1	0	EtOH/3.0	R.T	3.0	50:50	45
2	0.01, 0.31	EtOH/3.0	R.T	1.0	80:20	78
3	0.02, 0.62	EtOH/3.0	R.T	0.5	90:10	88
4	**0.03, 0.93**	**EtOH/3.0**	**R.T**	**0.25**	**100:00**	**98**
5	0.04, 1.24	EtOH/3.0	R.T	0.25	100:00	98
6	0.05, 1.55	EtOH/3.0	R.T	0.25	100:00	98
7	0.03, 0.93	EtOH/3.0	40	0.25	100:00	98
8	0.03, 0.93	EtOH/3.0	50	0.25	100:00	98
9	0.03, 0.93	EtOH/3.0	60	0.25	100:00	98
10	0.03, 0.93	EtOH/3.0	70	0.25	100:00	98
11	0.03, 0.93	EtOH/3.0	Reflux	0.25	100:00	98
12	0.03, 0.93	Solvent-free	R.T	0.50	70:30	62
13	0.03, 0.93	DMF	R.T	1.00	50:50	45
14	0.03, 0.93	H$_2$O	R.T	1.00	50:50	45
15	0.03, 0.93	CHCl$_3$	R.T	1.00	50:50	45
16	0.03, 0.93	CH$_3$CN	R.T	1.00	50:50	45
17	0.03, 0.93	CH$_2$Cl$_2$	R.T	1.00	50:50	45
18	0.03, 0.93	THF	R.T	1.00	50:50	45
19	0.03, 0.93	Toluene	R.T	1.00	50:50	45
20	0.03, 0.93	DMSO	R.T	1.00	60:40	55
21	0.03, 0.93	EtOAc	R.T	1.00	60:40	55
22	0.03, 0.93	EtOH/H$_2$O (2:1/v:v)[b]	R.T	1.00	90:10	88
23	0.03, 0.93	EtOH/1.0	R.T	1.00	80:20	78
24	0.03, 0.93	EtOH/2.0	R.T	1.00	90:10	88
25	0.03, 0.93	EtOH/4.0	R.T	0.25	100:00	98
26	0.03, 0.93	EtOH/5.0	R.T	0.25	100:00	98

Reaction conditions: 0.11 g *o*-PD (1.0 mmol), 0.2 cm^3 benzaldehyde (2.0 mmol), catalyst, solvent, and temperature

[a]Yield of isolated product

[b]2:1 volume ratio of EtOH and H$_2$O was used

time but also increases the selectivity and yield toward the synthesis of **3a** (Table 1, entries 2 and 3), which demonstrates the vital role of the nanocatalyst in the condensation reaction. In continuation, the addition of 0.03 g (0.93 mol% Cr) nanocatalyst showed its remarkable ability, entire selectivity, and 98% yield within a short reaction time (15 min) (Table 1, entry 4). Further increase in the amount of the nanocatalyst exerted no visible effect on the reaction process (Table 1, entries 5 and 6). Therefore, 0.03 g (0.93 mol% Cr) of the Fe$_3$O$_4$@SiO$_2$/Schiff-base/Cr(III) nanocatalyst was selected as the most suitable amount (Table 1, entry 4). Next, the effect of other solvents on the model reaction in the presence of nanocatalyst (0.03 g, 0.93 mol% Cr) at RT was examined. According to the obtained results, the model reaction in solvents like DMF, H$_2$O, CHCl$_3$, CH$_3$CN, CH$_2$Cl$_2$, THF, and toluene did not show good selectivity and the desired product **3a** was achieved with a 45% yield within 1 h (Table 1, entries 13–19). Also, the selectivity and yield increased slowly in the presence of DMSO and EtOAc, which results in a 55% yield (Table 1, entries 20 and 21). The solvent-free condition reached the selectivity of 70:30 (**3a**:**4a**) with a 62% yield. However, the favorable yield was not achieved (Table 1, entry 12). Although the tendency toward good selectivity (90:10) and yield (88%) was observed in the solution of EtOH/H$_2$O (2:1/*v*:*v*) (Table 1, entry 22), the excellent selectivity (100:00) and yield (98%) were achieved in EtOH (Table 1, entry 4). Therefore, EtOH was introduced as the best solvent for the synthesis of **3a** with 0.03 g of the nanocatalyst. In addition, the model reaction was carried out in different volumes of EtOH. Despite satisfactory results in the lower volumes (1.0 and 2.0 cm^3) of EtOH (Table 1, entries 23 and 24), 3.0 cm^3 of EtOH (Table 1, entry 4) and higher ones (Table 1, entries 25 and 26) revealed the profound influence on both the efficiency of the nanocatalyst and model reaction. Afterward, the temperature parameter was checked on the model reaction in the presence of the nanocatalyst (0.03 g, 0.93 mol% Cr) and EtOH (3.0 cm^3). Raising the temperature did not only exert any negative effect, but it also demonstrated the same results as one at RT (Table 1, entries 7–11). Based on the above-mentioned observations, the optimum conditions were considered as *o*–PD (**1a**, 1.0 mmol, 0.11 g), benzaldehyde (**2a**, 2.0 mmol, 0.2 cm^3), Fe$_3$O$_4$@SiO$_2$/Schiff-base/Cr(III) nanocatalyst (0.03 g, 0.93 mol% Cr), EtOH (3.0 cm^3), and RT conditions for the synthesis of 1-benzyl-2-phenyl-1*H*-benzo[*d*]imidazole (**3a**).

At the final stage of the optimization, the ability and efficiency of other Schiff-base ion metal complexes supported on the Fe$_3$O$_4$@SiO$_2$, and the role of bare Fe$_3$O$_4$ and Fe$_3$O$_4$@SiO$_2$ NPs as catalysts in the model reaction were investigated (Table 2). The complexes of Cu, Co, Ni, Zn, Cd, Pd, Mn, and Fe metal ions supported on Fe$_3$O$_4$@SiO$_2$ NPs did

Table 2 Catalytic performance of Fe$_3$O$_4$@SiO$_2$/Schiff-base/metal ion complexes, bare Fe$_3$O$_4$, and Fe$_3$O$_4$ in the synthesis of 1-benzyl-2-phenyl-1*H*-benzo[*d*]imidazole (**3a**)

Entry	Catalyst	Time/h	Selectivity 3a:4a	Yield[a]/%
1	Fe$_3$O$_4$@SiO$_2$/Schiff base/Cr(III)	0.25	100:00	98
2	Fe$_3$O$_4$@SiO$_2$/Schiff base/Cu(II)	1.0	50:50	45
3	Fe$_3$O$_4$@SiO$_2$/Schiff base/Co(II)	1.0	60:40	54
4	Fe$_3$O$_4$@SiO$_2$/Schiff base/Ni(II)	1.0	50:50	45
5	Fe$_3$O$_4$@SiO$_2$/Schiff base/Zn(II)	1.0	60:40	53
6	Fe$_3$O$_4$@SiO$_2$/Schiff base/Cd(II)	1.0	50:50	45
7	Fe$_3$O$_4$@SiO$_2$/Schiff base/Pd(II)	1.0	50:50	40
8	Fe$_3$O$_4$@SiO$_2$/Schiff base/Mn(II)	1.0	50:50	45
9	Fe$_3$O$_4$@SiO$_2$/Schiff base/Fe(II)	0.5	60:40	54
10	Fe$_3$O$_4$	24	60:40	50
11	Fe$_3$O$_4$@SiO$_2$	24	0	0

Reaction conditions: 0.11 g *o*–PD (1.0 mmol), 0.2 cm^3 benzaldehyde (2.0 mmol), 0.03 g catalyst, 3.0 cm^3 EtOH, and RT
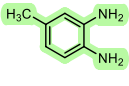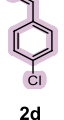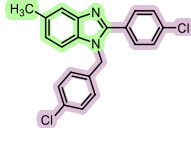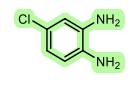
[a]Yield of isolated product
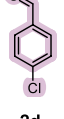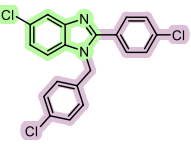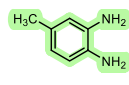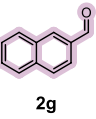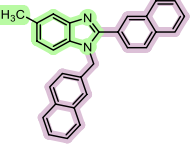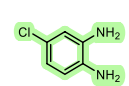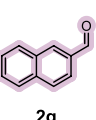
not perform efficiently as well as Cr(III) (Table 2, entries 2–9). The Fe$_3$O$_4$ was not able to catalyze the reaction well (Table 2, entry 10), and coating with the SiO$_2$ shell made it inactive as a catalyst (Table 2, entry 11). So, the Fe$_3$O$_4$@SiO$_2$/Schiff-base/Cr(III) was selected as a new, efficient, and magnetically heterogeneous nanocatalyst (Table 2, entry 1).

Having optimized the reaction conditions, we studied the efficiency of Fe$_3$O$_4$@SiO$_2$/Schiff-base/Cr(III) magnetic nanocatalyst in the synthesis of various 1,2-disubstituted benzimidazole compo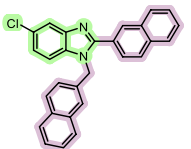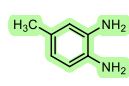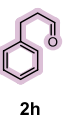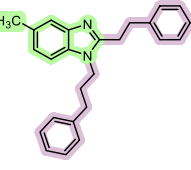unds by using different substituted *o*-PDs (**1a–1c**) and aldehydes (**2a–2h**). As depicted in Table 3, the desired products (**3a–3m**) were formed successfully within short reaction times (10–28 min) and with good to excellent yields (88–98%). As before mentioned, the condensation reaction between *o*–PD (**1a**) and benzaldehyde (**2a**) as the model starting materials was completed successfully within 15 min and 98% yield (Table 3, entry 1). The *o*–PD substrate bearing the CH$_3$ as the electron-donating group (**1b**) increases the nucleophilic attack rate toward the carbonyl group in benzaldehyde (**2a**), which resulted in a shorter reaction time and a higher amount of Turnover Frequency (TOF) (Table 3, entry 3). The reaction performed between *o*–PD (**1a**) and aldehydes containing electron-donating groups like *p*-CH$_3$ (**2b**) and *p*-N(CH$_3$)$_2$ (**2e**) afforded the products (**3b** and **3f**) in longer reaction times

Table 3 Fe$_3$O$_4$@SiO$_2$/Schiff-base/Cr(III)-catalyzed synthesis of 2-aryl-1-(arylmethyl)-1*H*-benzimidazole derivatives
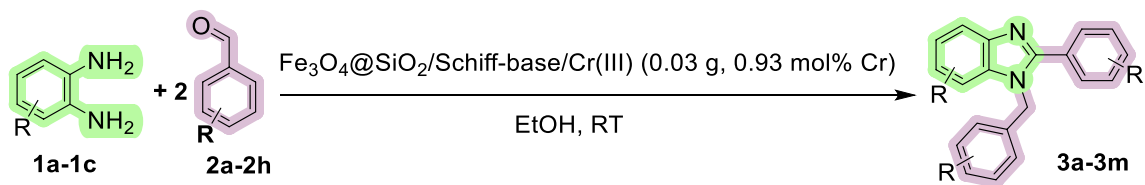
Entry	substrate	substrate	Product	Time/h	Yield[a]/%	TON[b]	TOF[c]/h^{-1}	M.p./°C [d] [Ref]
1	1a	2a	3a	0.25	98	105	422	129-131 (129-130 [44])
2	1a	2b	3b	0.37	96	103	279	126-129 (125-127 [44])
3	1b	2a	3c	0.17	96[e]	103	607	[60][f]
4	1a	2c	3d	0.20	90	97	484	Semi-solid [13][f]
5	1a	2d	3e	0.30	92	99	323	131-134 (131-135 [44])
6	1a	2e	3f	0.42	98	105	251	253-255 (252-253 [31])
7	1b	2e	3g	0.30	98[e]	105	351	New[g]
8	1a	2f	3h	0.30	88	95	315	149-151 (150-152 [25])

Table 3 (continued)

9	**1b**	**2d**	**3i**	0.25	94[e]	101	404	[60][f]
10	**1c**	**2d**	**3j**	0.43	92	99	230	130-132 New[g]
11	**1b**	**2g**	**3k**	0.30	90[e]	97	323	New[g]
12	**1c**	**2g**	**3l**	0.47	92	99	210	123-126 New[g]
13	**1b**	**2h**	**3m**	0.27	90[e]	97	359	Oil New[g]

Reaction conditions: *o*-PD (1.0 mmol), aldehyde (2.0 mmol), 0.03 g catalyst (0.93 mol% Cr), 3.0 cm³ EtOH, and RT

[a]Yield refers to isolated product

[b]Turnover number (mmol of product/mmol of catalyst)

[c]Turnover frequency (TON/time of reaction)

[d]The melting point of the product was compared to that in the literature unless otherwise stated

[e] The mixture of regio-isomers was obtained

[f]The spectroscopic data of the product was compared to that in the literature

[g]New compound was identified by spectroscopic data

and excellent yields (Table 3, entries 2 and 6). Also, the products (**3d** and **3e**) were obtained successfully from *o*–PD (**1a**) and aldehydes bearing electron-withdrawing groups like *m*-OCH₃ (**2c**) and *p*-Cl (**2d**) within shorter reaction times (Table 3, entries 4 and 5). The presence of electron donating substituent like *p*-N(CH₃)₂ in aldehyde (**2e**) increases the electron density of carbonyl group. However, the electron donating group like *m*-CH₃ in *o*–PD (**1b**) and the activating function of nanocatalyst on the carbonyl group in aldehyde led to the products (**3g**) within 18 min and 98% yield (Table 3, entry 7). The benzaldehyde with *p*-Cl substituent

(**2d**) was treated with the *o*-PDs containing *m*-CH₃ (**1b**) and -Cl (**1c**) substituents with 94 and 92% yields of the products (**3i** and **3j**), respectively (Table 3, entries 9 and 10). Also, 1-naphthaldehyde (**2 g**) attacked successfully by the *o*-PDs containing *m*-CH₃ (**1b**) and -Cl (**1c**) substituents led to the products (**3k** and **3l**) with 90 and 92% yields, respectively (Table 3, entries 11 and 12). The great merit of nanocatalyst was examined by using heteroaromatic and aliphatic aldehydes like thiophene-2-carbaldehyde (**2f**), and 3-phenylpropanal (**2h**) in the condensation reaction and the products (**3h** and **3m**) were gained with 88 and 90% yields (Table 3,

Scheme 3

Dibenzylidene-*o*-phenylenediamine (A)
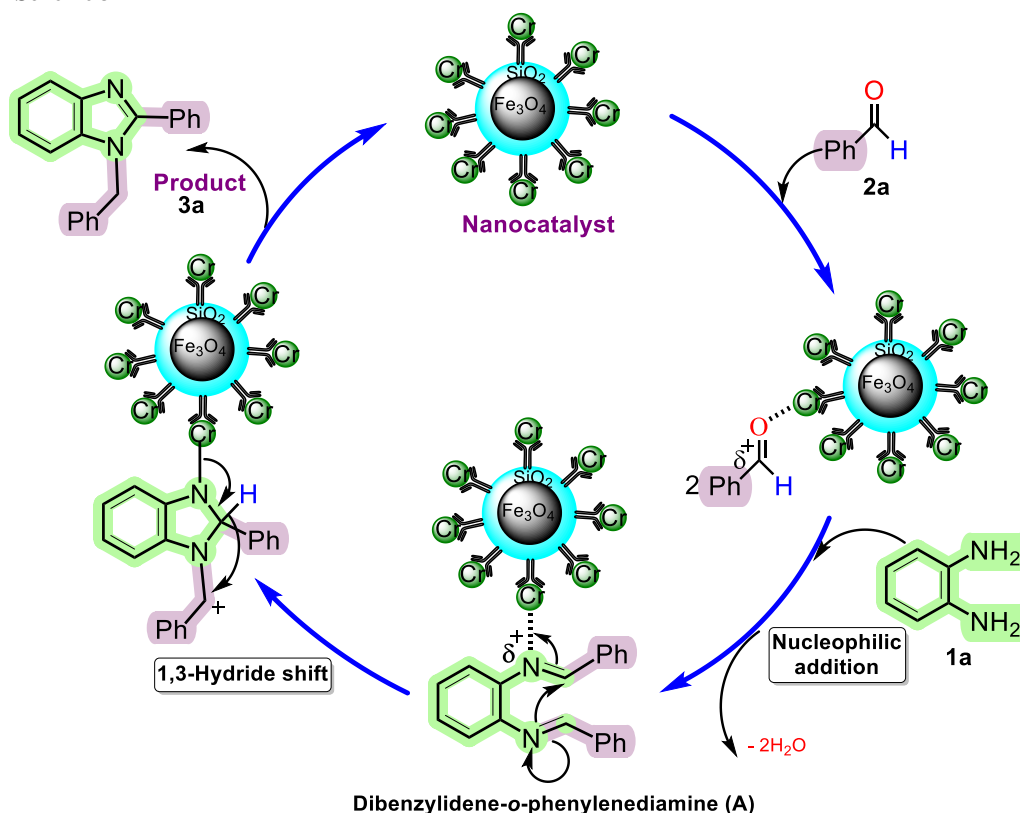
entries 8 and 13). These results offer the remarkable feature of the Fe₃O₄@SiO₂/Schiff-base/Cr(III) nanocatalyst in the condensation reaction for the synthesis of 1,2-disubstituted benzimidazoles.

A plausible mechanism of the condensation reaction between *o*–PD (**1a**) and benzaldehyde (**2a**) catalyzed by Fe₃O₄@SiO₂/Schiff-base/Cr(III) nanocatalyst is proposed in Scheme 3. Based on the reported acid-catalyzed reaction pathway in the literature [24, 38, 44, 61], the mechanism follows a tandem sequence of reactions. First, the oxygen of the carbonyl group is coordinated by the Cr NPs, which makes the carbon of the carbonyl group in benzaldehyde (**2a**) more electrophilic to undergo nucleophilic attack by *o*–PD (**1a**). The nucleophilic addition of *o*–PD (**1a**) to benzaldehyde (**2a**) results in the formation of dibenzylidene-*o*–PD (**A**) as an intermediate. Then, the presence of the nanocatalyst brings about a profound effect on intramolecular cyclization, which results in a five-membered ring. Finally, the mechanism is completed by the 1,3-hydride migration, which releases the nanocatalyst and makes 1-benzyl-2-phenyl-1*H*-benzo[*d*]imidazole product (**3a**) (Scheme 3).

Regarding the economic and environmental issues, the recyclability and reusability of the catalysts are of great importance [62]. We evaluated the ability of magnetically heterogeneous Fe₃O₄@SiO₂/Schiff-base/Cr(III) nanocatalyst which has been used efficiently in successive condensation

reactions. In this regard, the recyclability of the nanocatalyst was examined under the optimized model reaction conditions. The condensation reaction between *o*–PD (**1a**, 1.0 mmol, 0.11 g) and benzaldehyde (**2a**, 2.0 mmol, 0.2 cm³) was catalyzed by the nanocatalyst (0.03 g, 0.93 mol% Cr) in EtOH (3.0 cm³) at RT. The nanocatalyst was separated by an external magnetic field from the reaction mixture after the completion of the reaction, which shows not only the magnetic behavior of the nanocatalyst but the easy and simple operation for retrieving the nanocatalyst, too (Fig. 6a). Then, the nanocatalyst was washed with EtOH and dried at 80 °C in an oven for 1 h before being used for the next following reactions under the optimized conditions. As shown in Fig. 6b, the recovered nanocatalyst revealed consistent activity in the condensation reaction for eight runs. The favorable yields of the isolated product indicate high stability and recyclability of the Fe₃O₄@SiO₂/Schiff-base/Cr(III) nanocatalyst up to seven cycles. A slight and gradual decrease can be related to the small leaching of the Cr NPs from the nanocatalyst. The results obtained from the ICP analysis of the recovered nanocatalyst showed negligible leaching for Cr from 0.8% after the first run to 1.2% after the eighth one. Furthermore, the hot filtration test was done to confirm the heterogeneity of the nanocatalyst without considerable leaching of Cr NPs. Having started the reaction with optimized conditions, we magnetically separated
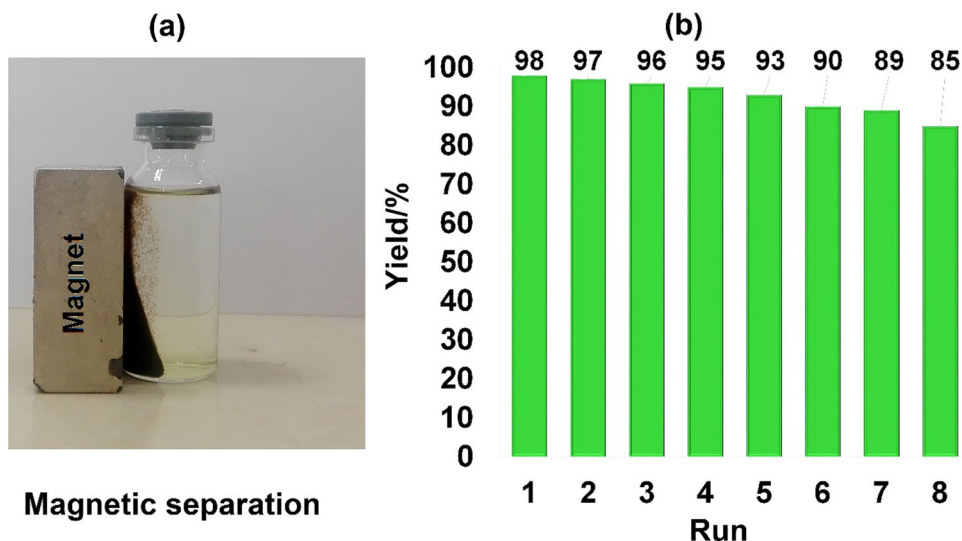
the nanocatalyst from the reaction mixture after 5 min and let the reaction be continued for up to 15 min. Thin Layer Chromatography (TLC) monitoring during the reaction and the low yield of the isolated product after the reaction confirmed little leaching of Cr NPs and recognized the Fe₃O₄@SiO₂/Schiff-base/Cr(III) NPs as stable, heterogeneous, and magnetic nanocatalyst for the condensation reaction.

The morphology, size, and chemical structure of the Fe₃O₄@SiO₂/Schiff-base/Cr(III) nanocatalyst were determined by FE-SEM, DLS, FT-IR, and XRD after the eighth run (Fig. 7). The surface morphology and spherical shape of the NPs in the recovered nanocatalyst did not undergo considerable change after being used in the recycling reactions, which shows the stability and nano identity of the nanocatalyst (Fig. 7a). The result of the DLS analysis reports

Fig. 7 a FE-SEM image; **b** DLS image; **c** XRD pattern; and **d** FT-IR spectrum of Fe₃O₄@SiO₂/Schiff-base/Cr(III) after seven reaction cycles
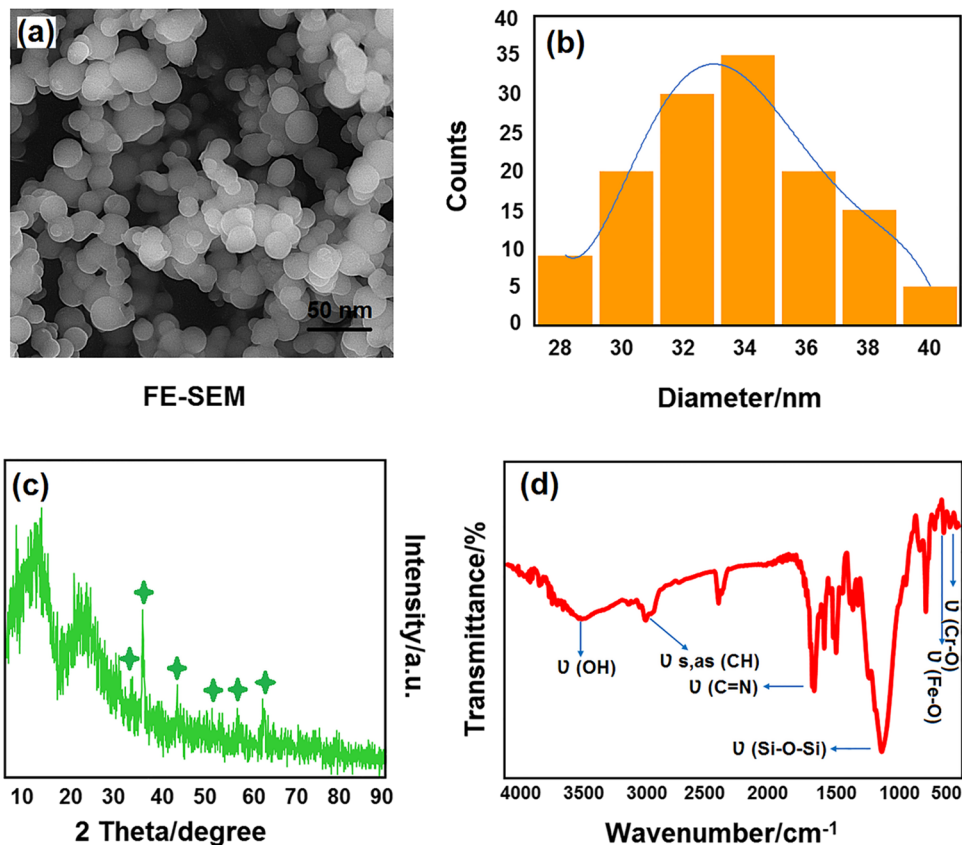
a slight increase in the size of the reused nanocatalyst with an average size of 34 nm compared to that of fresh nanocatalyst with a mean size of 32 nm (Fig. 5i), which indicates a little aggregation of the NPs during the recycling reactions (Fig. 7b). As shown in Fig. 7c, the XRD characteristic peaks presented in the reused nanocatalyst are similar to those in the fresh nanocatalyst (Fig. 2h), which confirms the successful functionalization of Fe_3O_4 NPs along with maintaining the crystalline structure during the reusing process. The FT-IR spectrum of the recovered nanocatalyst also presents the main vibration bands at 520, 580, 1160, and 1620 cm^{-1} related to the Cr–O, Fe–O, Si–O-Si, and C=N bonds, respectively (Fig. 7d). These bands being similar in both fresh (Fig. 2e) and recovered nanocatalyst verify the maintained structure of the nanocatalyst. As for these observations, the $Fe_3O_4@SiO_2$/Schiff-base/Cr(III) as a stable nanocatalyst performs well in the catalytic and recovery process.

The synthesis of 1,2-disubstituted benzimidazoles has been reported by different catalysts, which a brief review of the reaction conditions of some of them have been displayed in Table 4. Although Zn-proline was reported as an inexpensive Lewis acid catalyst to prepare 1,2-disubstituted benzimidazoles, which it catalyzed the reaction in a longer reaction time and led to a lower TOF, consequently (Table 4, entry 1). Erbium(III) trifluoromethanesulfonate [Er(OTf)$_3$] catalyzed the condensation reaction efficiently within a short reaction time and, solvent-free conditions. However, the high amount of the catalyst, high temperature along with the not mentioned recycling result is of high consideration (Table 4, entry 2). The green and reusable iron(III) phosphate (FePO$_4$) showed satisfactory results in the synthesis of 1,2-disubstituted benzimidazoles, but the desired product was not

formed when using aliphatic aldehydes (Table 4, entry 3). Applying a large amount of catalyst and high temperature contributed to the synthesis of 1,2-disubstituted benzimidazoles catalyzed by the ZrO_2-supported β-cyclodextrin nanoparticles (ZrO_2-β-CD) with the cost of longer reaction time and lower TOF (Table 4, entry 4). Furthermore, nano indium oxide (In_2O_3), and alumina-sulfuric acid as recyclable catalysts were able to catalyze the condensation reaction at a lower reaction rate and also TOF (Table 4, entries 5 and 6). Moderate reaction conditions were used in the condensation reaction catalyzed by silica gel-supported trichloroacetic acid (SiTCA), in which the less recycling number and amount of TOF are observable (Table 4, entry 7). The catalytic system of ytterbium-supported mesoporous silica nanoparticles (Yb@l-MSNs) provided acceptable results within 1 h reaction time (Table 4, entry 8). Moreover, the synthesis of 1,2-disubstituted benzimidazoles was reported in the presence of erbium in a pentanuclear coordination cluster [Er$_5$(LH)$_4$(acac)$_4$(μ$_3$-O)(μ$_3$-OH)(H$_2$O)$_2$]·5H$_2$O as a catalyst, which leads to moderate to good yields in products at high temperature. Although this catalyst demonstrated high TOF, its recyclability was not reported (Table 4, entry 9). Also, 1,2-disubstituted benzimidazole derivatives were produced by the heterogeneous cobalt ferrite magnetic nanocomposite [CoFe$_2$O$_4$/Cu(OH)$_2$] as a catalyst. In this catalytic system, a short reaction time did not cause a high amount of TOF due to using a high amount of the catalyst (Table 4, entry 10). The reaction conditions are not favorable for yttrium(III) chloride (YCl$_3$) as a catalyst, which required a high amount of the catalyst, and a long reaction time with no recycling report (Table 4, entry 11). Also, bismuth triflate [Bi(OTf)$_3$] was efficiently used as a readily available catalyst

Table 4 A brief report of catalysts and $Fe_3O_4@SiO_2$/Schiff-base/Cr(III) for the preparation of 2-phenyl-1-(phenylmethyl)-1*H*-benzimidazole

Entry	Catalyst/g, mol%	Conditions	Time/h	Yield/%	TON	TOF/h^{-1}	Cycle	References
1	Zn-Proline (5.0)	H$_2$O/25 °C	2.0	92	18.4	9.2	3	[24]
2	Er(OTf)$_3$ (10.0)[b]	Solvent-free/80 °C	0.03	91	4.5	151.7	–	[36]
3	FePO$_4$ (2.0)	Solvent-free/RT	0.33	90	45.0	136.4	4	[61]
4	ZrO$_2$-β-CD (40.0)	Solvent-free/100 °C	1.0	93	2.3	2.3	4	[34]
5	Nano In$_2$O$_3$ (5.0)	EtOH/H$_2$O (2:1)/60 °C	2.0	89	17.8	8.9	3	[30]
6	Alumina-sulfuric acid (3.0)	EtOH/RT	3.0	85	28.3	9.4	6	[63]
7	SiTCA (6.5)	EtOH /50 °C	0.2	93	14.3	71.5	3	[64]
8	Yb@l-MSNs (2.4)	EtOH/H$_2$O (2:1)/RT	1.0	80	33.3	33.3	4	[39]
9	Er(III) cluster (0.6)	Solvent-free/120 °C	0.17	91	75.8	446.1	–	[10]
10	CoFe$_2$O$_4$/Cu (OH)$_2$ (5.0)[b]	Solvent-free/100 °C	0.33	90	18.0	54.5	2	[43]
11	YCl$_3$ (10.0)	Solvent-free/RT	8.0	99	9.9	1.23	–	[29]
12	Bi(OTf)$_3$ (10.0)	H$_2$O/RT	0.05	97	9.7	194	2	[25]
26	Fe$_3$O$_4$@SiO$_2$/Schiff-base/Cr(III) (0.93)	EtOH/RT	0.25	98	105.4	421.6	7	This work

[a]Benzaldehyde (2.0 mmol) and *o*–PD (1.0 mmol) were used as substrates unless otherwise stated

[b]4-Methoxybenzaldehyde (2.0 mmol) and *o*–PD (1.0 mmol) were used for the recycling process

in the condensation reaction. However, the reaction did not materialize unless a large amount of catalyst was applied (Table 4, entry 12). In our catalytic system, the low amount of nanocatalyst (0.03 g, 0.93 mol% Cr), safe reaction conditions (EtOH, RT), and short reaction time (15 min) resulted in excellent yield and high TOF. The reusability of the nanocatalyst significantly shows the potential ability and stability of the nanocatalyst (Table 4, entry 13). Therefore, $Fe_3O_4@$ SiO_2/Schiff-base/Cr(III) is considered as an advanced, economical, capable, and nanomagnetic catalyst in the synthesis of 1,2-disubstituted benzimidazoles.

Conclusion

In conclusion, we have synthesized the $Fe_3O_4@SiO_2$/Schiff-base/Cr(III) NPs as novel, efficient, heterogeneous, and magnetically recoverable nanocatalyst. The nanocatalyst was identified by FT-IR, XRD, VSM, TGA, EDX, TEM, FE-SEM, and DLS characterization techniques, which shows the successful functionalization, magnetic property, thermal stability, nanosized particles along with unique spherical structure. The Cr(III) nanocatalyst performed effectively in the synthesis of 1,2-disubstituted benzimidazole derivatives using EtOH as a green solvent at ambient temperature. This safe catalytic system made the products within short reaction times with desirable yields. The acidic nature of the nanocatalyst increased the chemoselective tendency toward the 1,2-disubstituted production. The high reusability of the nanocatalyst was affirmed in consecutive reactions. This catalytic approach offers remarkable features including (a) facile operation, (b) easy magnetically separation, (c) high productivity, and (d) sustainability and great recyclability, which considers the $Fe_3O_4@SiO_2$/Schiff-base/Cr(III) nanocatalyst an attractive candidate for the synthesis of 1,2-disubstituted benzimidazoles.

Experimental

All solvents and chemicals were purchased from Fluka, Merck, and Aldrich chemical companies and were applied with no more purification. The spectra of ^1H NMR at 250 MHz and ^{13}C NMR at 62.9 MHz were reported by a Bruker Avance DPX-250 spectrometer in $CDCl_3$ or DMSO-d_6 using tetramethylsilane (TMS) as an internal reference. The FT-IR spectra of the materials were recorded on a Shimadzu FT-IR 8300 spectrophotometer. The phase composition and the crystalline structure of MNPs were investigated by Bruker AXS D8-Advance X-ray diffractometer with Cu Kα radiation ($\lambda = 1.5418$). The magnetization of NPs was measured on a BHV-55 VSM, and the thermal stability of the NPs was determined by TGA using a NETZSCH STA 409 PC/PG. The characterization of elements was conducted by EDX spectroscopy. The TEM images were

recorded using a Philips EM208 transmission electron microscope operated at 80 kV accelerating voltage. The morphological characterization of the NPs was analyzed using FE-SEM by HITACHI S-4160. The specific surface area of the nanocatalyst was determined through BET analysis measured on a Micromeritics ASAP 2000 instrument at 196 °C. The size distribution of the NPs was measured by the DLS technique using a HORIBA-LB 550 particle size analyzer. The loading amount of Cr in the nanocatalyst and leaching amount was measured by the Varian Vista-pro ICP analyzer. The purity of the products and the reaction progress were determined and monitored performed by TLC on a silica-gel polygram SILG/UV 254 plate.

General procedure for the synthesis of Fe₃O₄@SiO₂ MNPs

Fe_3O_4 NPs were synthesized through the coprecipitation method based on our previous study [49]. First, the mixture of 1.3 g $FeCl_3 \cdot 6H_2O$ (4.0 mmol), 0.9 g $FeCl_2 \cdot 4H_2O$ (4.5 mmol), and 1.0 g polyvinyl alcohol (PVA 15000) as a surfactant was mechanically stirred in a beaker containing 30.0 cm³ deionized water at 80 °C for 0.5 h. Hexamethylenetetramine (HMTA, 1.0 mol/dm³) was then added dropwise with vigorous stirring to produce a black solid product until the reaction medium reached pH 10. After heating at 60 °C for 2 h, the black magnetic Fe_3O_4 product was collected by a magnet followed by washing three times with ethanol and deionized water. The core–shell $Fe_3O_4@SiO_2$ MNPs were synthesized by a modified Stöber method [49]. Fe_3O_4 (0.5 g, 2.1 mmol) was added to a beaker containing 50.0 cm³ EtOH, 5.0 cm³ deionized water, and 0.2 cm³ TEOS (1.0 mmol), followed by dropwise addition of 5.0 cm³ NaOH 10%w. After stirring at RT for 0.5 h, the $Fe_3O_4@SiO_2$ product was washed with ethanol and deionized water and dried at 80 °C for 10 h.

General procedure for the synthesis of Fe₃O₄@SiO₂/ Schiff-base/Cr(III)

The prepared $Fe_3O_4@SiO_2$ is ready to support the Schiff-base complex of Cr(III). In advance, the Schiff base ligand is synthesized followed by anchoring of the Cr metal ions. In this regard, the reaction between 0.23 cm³ APTES (1.0 mmol) and 0.11 cm³ salicylaldehyde (1.0 mmol) in 50.0 cm³ EtOH (0.86 mmol) at RT for 6 h led to the formation of Schiff base ligand. The yellow solid product was washed with ethanol and dried in vacuum [49]. Afterward, the Schiff-base complex of Cr(III) was prepared through the reaction between 0.72 g $Cr(OAc)_3$ (1.0 mmol) and 0.65 g Schiff-base ligand (2.0 mmol) in 25.0 cm³ EtOH (0.43 mmol) under reflux conditions, which resulted in a green-color product. Finally, heating the mixture of Schiff-base complex of 0.7 g Cr(III) (1.0 mmol) and 2.0 g $Fe_3O_4@$

SiO$_2$ in 10.0 cm^3 EtOH (0.17 mmol) under reflux conditions contributed to the formation of Fe$_3$O$_4$@SiO$_2$/Schiff-base/Cr(III) nanocatalyst after 12 h. The nanocatalyst was separated by an external magnet, washed with ethanol and water, and dried at 80 °C for 6 h.

General procedure for the synthesis of 1,2-disubstituted benzimidazole derivatives catalyzed by Fe$_3$O$_4$@SiO$_2$/Schiff-base/Cr(III)

In a round bottom flask, a mixture of *o*–PD (1.0 mmol), benzaldehyde (2.0 mmol), and 0.03 g Fe$_3$O$_4$@SiO$_2$/Schiff-base/Cr(III) nanocatalyst (0.93 mol% Cr) in 3.0 cm^3 EtOH was stirred at RT for the specific time (see Table 3). After completion of the reaction as monitored by TLC, the nanocatalyst was easily separated from the reaction mixture by an external magnet. Having been washed with ethanol and water three times, and dried at 80 °C for 1 h, the nanocatalyst was reapplied in the successive cycles of reaction. The residue mixture was purified by column chromatography (silica gel) using hexane and ethyl acetate or crystallization to afford the pure product. All the products were identified by ^{1}H NMR and ^{13}C NMR and were confirmed by comparing the spectral data and melting points with those in the literature.

4-[1-[4-(Dimethylamino)benzyl]-5-methyl-1*H*-benzo[*d*]-imidazol-2-yl]-*N*,*N*-dimethylaniline and 4-[1-[4-(dimethylamino)benzyl]-6-methyl-1*H*-benzo[*d*]imidazol-2-yl]-*N*,*N*-dimethylaniline (3g and 3g′, C$_{25}$H$_{28}$N$_4$)

Pale yellow solid (isomeric mixture); yield: 98% (isomer ratio: 57:43); ^{1}H NMR (250 MHz, DMSO-d_6): δ = 2.35 (s, 3.18H, CH$_3$), 2.37 (s, 2.82H, CH$_3$), 2.80 (s, 6H, CH$_3$), 2.82 (s, 6H, CH$_3$), 2.93 (s, 6H, CH$_3$), 2.95 (s, 6H, CH$_3$), 5.35 (s, 2.11H, CH$_2$), 5.37 (s, 1.89H, CH$_2$), 6.59–6.64 (m, 4H, Ar–H), 6.74–6.87 (m, 8H, Ar–H), 6.99–7.03 (m, 2H, Ar–H), 7.14–7.16 (bs, 2H, Ar–H), 7.47–7.59 (m, 6H, Ar–H) ppm; ^{13}C NMR (62.9 MHz, DMSO-d_6): δ = 21.4, 39.7, 40.0, 46.9, 46.9, 110.4, 111.6, 112.5, 118.0, 123.3, 124.2, 126.7, 129.7, 131.1, 136.1, 140.5, 141.1, 149.6, 150.7 ppm; FT-IR (KBr): $\overline{V}$ = 2916 (w), 2800 (w), 1612 (s), 1365 (m) cm^{-1}.

5-Chloro-1-(4-chlorobenzyl)-2-(4-chlorophenyl)-1*H*-benzimidazole (3j, C$_{20}$H$_{13}$Cl$_3$N$_2$)

Pale yellow solid; yield: 92%; m.p.: 130–132 °C; ^{1}H NMR (250 MHz, DMSO-d_6): δ = 5.58 (bs, 2H, CH$_2$), 6.95–6.98 (d, *J* = 7.5 Hz, 2H, Ar–H), 7.26–7.34 (m, 3H, Ar–H), 7.50–7.59 (m, 3H, Ar–H), 7.69–7.78 (m, 3H, Ar–H) ppm; ^{13}C NMR (62.9 MHz, DMSO-d_6): δ = 46.8, 47.0, 111.0, 112.5, 118.8, 120.7, 122.8, 123.1, 126.9, 127.4, 128.0, 128.3, 128.8, 129.0, 130.8, 132.1, 134.7, 135.0, 135.4, 143.3, 153.5 ppm; FT-IR (KBr): $\overline{V}$ = 3062 (m), 2923 (m), 1650 (m), 1296 (w) cm^{-1}.

5-Methyl-2-(naphthalen-2-yl)-1-(naphthalen-2-ylmethyl)-1*H*-benzimidazole and 6-methyl-2-(naphthalen-2-yl)-1-(naphthalen-2-ylmethyl)-1*H*-benzo[*d*]imidazole (3k and 3k′, C$_{29}$H$_{22}$N$_2$)

Pale yellow solid (isomeric mixture); yield: 90% (isomer ratio: 60:40); ^{1}H NMR (250 MHz, CDCl$_3$): δ = 2.40 (s, 3.60H, CH$_3$), 2.50 (s, 2.40H, CH$_3$), 5.58 (bs, 4H, CH$_2$), 7.05 (s, 2H, ArH), 7.10–7.18 (m, 2H, Ar–H), 7.24–7.30 (t, *J* = 7.5 Hz, 2H, Ar–H), 7.43–7.49 (m, 8H, Ar–H), 7.53 (s, 2H, Ar–H), 7.67–7.72 (m, 4H, Ar–H), 7.81–7.86 (m, 12H, Ar–H), 8.17 (s, 2H, Ar–H) ppm; ^{13}C NMR (62.9 MHz, CDCl$_3$): δ = 21.6, 21.9, 48.6, 48.7, 110.1, 110.3, 119.5, 119.8, 123.9, 124.5, 124.7, 126.1, 126.2, 126.6, 127.1, 127.4, 127.7, 127.9, 128.5, 129.1, 132.5, 132.8, 132.9, 133.3, 133.4, 133.6, 134.1, 136.6, 141.45, 143.6, 153.8 ppm; FT-IR (KBr): $\overline{V}$ = 3047 (m), 2916 (m), 1650 (m), 1272 (w) cm^{-1}.

5-Chloro-2-(naphthalen-2-yl)-1-(naphthalen-2-ylmethyl)-1*H*-benzimidazole (3l, C$_{28}$H$_{19}$ClN$_2$)

Yellow solid; yield: 92%; m.p.: 123–126 °C; ^{1}H NMR (250 MHz, CDCl$_3$): δ = 5.63 (bs, 2H, CH$_2$), 7.17–7.18 (m, 2H, Ar–H), 7.25–7.28 (d, *J* = 7.5 Hz, 1H, Ar–H), 7.49–7.51 (m, 5H, Ar–H), 7.71–7.75 (m, 2H, Ar–H), 7.85–7.90 (m, 6H, Ar–H), 8.19 (s, 1H, Ar–H) ppm; ^{13}C NMR (62.9 MHz, CDCl$_3$): δ = 49.0, 111.4, 119.8, 123.6, 123.7, 124.7, 125.9, 126.4, 126.8, 126.8, 127.4, 127.8, 127.9, 128.4, 128.6, 128.7, 129.3, 129.4, 132.9, 132.9, 133.4, 133.5, 133.8, 134.9, 144.2, 155.5 ppm; FT-IR (KBr): $\overline{V}$ = 3055 (m), 2923 (s), 1650 (m), 1272 (w) cm^{-1}.

5-Methyl-2-phenethyl-1-(3-phenylpropyl)-1*H*-benzimidazole and 6-methyl-2-phenethyl-1-(3-phenylpropyl)-1*H*-benzo[*d*]imidazole (3 m and 3m′, C$_{25}$H$_{26}$N$_2$)

White oil (isomeric mixture); yield: 90% (isomer ratio: 69.5:30.5); ^{1}H NMR (250 MHz, CDCl$_3$): δ = 2.03 (q, *J* = 7.5 Hz, 4H, CH$_2$), 2.48 (s, 3H, CH$_3$), 2.49 (s, 3H, CH$_3$), 2.62–2.69 (m, 4H, CH$_2$), 3.01–3.07 (t, *J* = 7.5 Hz, 4H, CH$_2$), 3.17–3.23 (t, *J* = 7.5 Hz, 4H, CH$_2$), 3.93 (t, *J* = 7.5 Hz, 4H, CH$_2$), 6.96–7.09 (m, 4H, Ar–H), 7.13–7.19 (m, 8H, Ar–H), 7.24–7.35 (m, 12H, Ar–H), 7.56–7.66 (m, 2H, Ar–H) ppm; ^{13}C NMR (62.9 MHz, CDCl$_3$): δ = 21.6, 21.8, 29.6, 30.9, 32.9, 34.1, 34.2, 42.6, 42.8, 108.8, 109.3, 118.7, 119.0, 123.4, 123.6, 126.4, 128.3, 128.3, 128.4, 128.6, 128.6, 131.6, 132.0, 140.3, 140.9, 140.9, 142.7, 153.9 ppm; FT-IR (KBr): $\overline{V}$ = 3082 (m), 2954 (m), 1620 (m), 1261 (m) cm^{-1}.

References

1. Khaliel S, Eswayah A, Aburmila F (2020) Pharmaceuticals 13:18
2. Florio R, Carradori S, Veschi S, Brocco D, Di Genni T, Cirilli R, Casulli A, Cama A, De Lellis L (2021) Pharmaceuticals 14:372
3. Sahoo MB, Banik KB, Mazaharunnisa Rao SN, Raju B (2019) Curr Microw Chem 6:23
4. Ganie MA, Dar MA, Khan AF, Dar AB (2019) Mini Rev Med Chem 19:1292
5. Pardeshi VA, Pathan S, Bhargava A, Chundawat NS, Singh GP (2021) Egypt J Basic Appl Sci 8:330
6. Guarda PM, Gualberto LdS, Mendes DB, Guarda EA, da Silva JEC (2020) J Environ Sci Health B 55:783
7. Tie-Gang R, Hong-Bin C, Jing-Lai Z, Wei-Jie L, Jia G, Li-Rong Y (2012) J Fluoresc 22:201
8. Milani JLS, Bezerra WDA, Valdo AKSM, Martins FT, Camargo LTFDM, Carvalho-Silva VH, dos Santos SS, Cangussu D, das Chagas RP (2019) Polyhedron 173:114134
9. Yang D, An B, Wei W, Tian L, Huang B, Wang H (2015) ACS Comb Sci 17:113
10. Sarkar A, Jana S, Nayek HP (2021) Appl Organomet Chem 35:e6200
11. Senapak W, Saeeng R, Jaratjaroonphong J, Promarak V, Sirion U (2019) Tetrahedron 75:3543
12. Putta RR, Chun S, Lee SB, Oh DC, Hong S (2020) Front Chem 8:429
13. Das K, Mondal A, Srimani D (2018) J Org Chem 83:9553
14. Xie C, Han X, Gong J, Li D, Ma C (2017) Org Biomol Chem 15:5811
15. Blatch AJ, Chetina OV, Howard JAK, Patrick LGF, Smethurst CA, Whiting A (2006) Org Biomol Chem 4:3297
16. Yeong KY, Alia MA, Ang CW, Tan SC, Osman H (2014) Tetrahedron Lett 55:4697
17. Zou B, Yuan Q, Ma D (2007) Angew Chem Int Ed 46:2598
18. Chen Y, Xu F, Sun Z (2017) RSC Adv 7:44421
19. Thapa P, Palacios PM, Tran T, Pierce BS, Foss FW (2020) J Org Chem 85:1991
20. Li A, Li C, Yang T, Yang Z, Liu Y, Li L, Tang K, Zhou C (2021) J Org Chem 84:16262
21. Kommi DN, Jadhavar PS, Kumar D, Chakraborti AK (2013) Green Chem 15:798
22. Brain CT, Brunton SA (2002) Tetrahedron Lett 43:1893
23. Ma Y, Xiong R, Feng Y, Zhang X, Xiong Y (2020) Tetrahedron 76:131474
24. Ravi V, Ramu E, Vijay K, Rao AS (2007) Chem Pharm Bull 55:1254
25. Yadav JS, Reddy BVS, Premalatha K, Shankar KS (2008) Can J Chem 86:124
26. Beheshtiha YS, Heravi MM, Saeedi M, Karimi N, Zakeri M, Tavakoli-Hossieni N (2010) Synth Commun 40:1216
27. Azarifar D, Mojgan P, Maleki B, Mehrangiz S, Nejat R (2010) J Serbian Chem Soc 75:1881
28. Bahrami K, Khodaei MM, Nejati A (2010) Green Chem 12:1237
29. Zhang LJ, Xia J, Zhou YQ, Wang H, Wang SW (2012) Synth Commun 42:328
30. Santra S, Majee A, Hajra A (2012) Tetrahedron Lett 53:1974
31. Mohammadi Ziarani G, Badiei A, Shakiba Nahad M, Ghadim Alizadeh S (2012) J Nanostruct 2:213
32. Durgareddy G, Ravikumar R, Ravi S, Adapa S (2013) J Chem Sci 125:175
33. Samuthirarajan S, Kumarraja M (2014) Tetrahedron Lett 55:1971
34. Girish YR, Sharath Kumar KS, Thimmaiah KN, Rangappa KS, Shashikanth S (2015) RSC Adv 5:75533
35. Sharma H, Kaur N, Singh N, Jang DO (2015) Green Chem 17:4263
36. Herrera Cano N, Uranga JG, Nardi M, Procopio A, Wunderlin DA, Santiago AN (2016) Beilstein J Org Chem 12:2410
37. Yu ZY, Zhou J, Fang QS, Chen L, Song ZB (2016) Chem Pap 70:1293
38. Pogula J, Laha S, Likhar P (2017) Catal Lett 147:2724
39. Samanta PK, Banerjee R, Richards RM, Biswas P (2018) Appl Organomet Chem 32:e4507
40. Tahanpesar E, Tavakkoli H, Hadikhani S (2019) Russ J Org Chem 55:1217
41. Kathing C, Singh NG, World Star Rani J, Nongrum R, Nongkhlaw R (2020) Russ J Org Chem 56:1628
42. Bonacci S, Iriti G, Mancuso S, Novelli P, Paonessa R, Tallarico S, Nardi M (2020) Catalysts 10:845
43. Anjaneyulu B, Dharma Rao GB, Nagakalyan S (2021) J Saudi Chem Soc 25:101394
44. Jamatia R, Saha M, Pal AK (2014) RSC Adv 4:12826
45. Maleki A, Ghamari N, Kamalzare M (2014) RSC Adv 4:9416
46. Alterary SS, AlKhamees A (2021) Green Process Synth 10:384
47. Eslahi H, Sardarian AR, Esmaeilpour M (2021) ChemistrySelect 6:1984
48. Azadi S, Sardarian AR, Esmaeilpour M (2021) Monatsh Chem 152:809
49. Esmaeilpour M, Sardarian AR, Javidi J (2012) Appl Catal A: Gen 445–446:359
50. Esmaeilpour M, Javidi J (2015) J Chin Chem Soc 62:614
51. Esmaeilpour M, Sardarian AR, Javidi J (2014) J Organomet Chem 749:233
52. Sarkheil M, Lashanizadegan M (2017) Appl Organomet Chem 31:e3726
53. Ebrahimiasl H, Azarifar D (2020) Appl Organomet Chem 34:e5359
54. Sardarian AR, Kazemnejadi M, Esmaeilpour M (2021) Appl Organomet Chem 35:e6051
55. Sardarian AR, Zohourian-Mashmoul N, Esmaeilpour M (2018) Monatsh Chem 149:1101
56. Kallmeier F, Fertig R, Irrgang T, Kempe R (2020) Angew Chem Int Ed 59:11789
57. Huang Y, Iwama T, Rawal VH (2000) J Am Chem Soc 122:7843
58. Gao X, Hall DG (2003) J Am Chem Soc 125:9308
59. Nieves-Quinones Y, Paniak TJ, Lee YE, Kim SM, Tcyrulnikov S, Kozlowski MC (2019) J Am Chem Soc 141:10016
60. Shadab, Gargi D, Motahar SK, Debasis B, Arshad A (2021) Inorg Chem 60:16042
61. Behbahani FK, Ziaei P (2012) Chin J Chem 30:65
62. Hu X, Yip ACK (2021) Front Catal 1:667675
63. Pramanik A, Roy R, Khan S, Ghatak A, Bhar S (2014) Tetrahedron Lett 55:1771
64. Kumar B, Smita K, Kumar B, Cumbal L (2014) J Chem Sci 126:1831